GPS Solutions (2026) 30:113
https://doi.org/10.1007/s10291-026-02078-w

RESEARCH

Improving GNSS-IR sea level retrievals using WinLSP with damping-aware height-rate correction and normalized IRLS

Cemali Altuntas[1,2] · Simon D. P. Williams[2] · Nursu Tunalioglu[1]

Received: 29 September 2025 / Accepted: 30 March 2026

Abstract
GNSS Interferometric Reflectometry (GNSS-IR) provides an independent and cost-effective approach for monitoring coastal sea level, but current methods still have important limitations. The classical height-rate correction relies on uniform weighting, which neglects amplitude decay effects, while the WinLSP framework applies bisquare weights directly to unscaled residuals, leading to inconsistent behavior across datasets. We introduced two methodological refinements, a damping-aware height-rate correction that accounts for amplitude decay caused by sea surface roughness and a normalized iteratively reweighted least squares (IRLS) strategy that stabilizes regression through robust residual scaling. Simulation experiments showed that the damping-aware correction reduced systematic errors by up to 50% under strong damping conditions. Real data analyses using one-month datasets from three coastal stations (ALTG, BRST, SHRN) confirmed the improvements. RMS errors decreased from 47.5 to 21.6 cm at ALTG, from 21.9 to 15.5 cm at BRST, and from 24.2 to 17.0 cm at SHRN, while correlations with tide gauges exceeded 99%. Overall, the results demonstrate the effectiveness of the refinements in reducing errors and improving GNSS-IR sea level retrievals across different coastal environments.

Keywords Damping effect · GNSS Interferometric Reflectometry (GNSS-IR) · Sea level · Windowed Lomb-Scargle Periodogram (WinLSP)

Introduction

Global Navigation Satellite Systems Interferometric Reflectometry (GNSS-IR) has become an important technique for monitoring environmental variables, such as snow depth (Larson et al. 2009; Altuntas et al. 2022), soil moisture (Larson et al. 2008; Altuntas and Tunalioglu 2020), sea ice thickness (Regmi et al. 2022), significant wave height (Roggenbuck et al. 2019), etc., as well as sea level (Larson et al. 2017; Wang et al. 2019). By analyzing multipath signals recorded at coastal GNSS stations, the method can provide sea level estimates that are independent of conventional tide gauges and complementary to satellite altimetry. The key idea is to extract the oscillation frequency in the signal-to-noise ratio (SNR) data, which is directly related to the reflector height. This feature makes GNSS-IR a practical and cost-effective approach for continuous sea level monitoring.

In the classical form, GNSS-IR assumes a constant reflector height during a satellite pass. However, in coastal regions the surface often changes within short time intervals, which shifts the frequency of the observed oscillations. To address this, several strategies have been proposed. The height-rate (h-rate) correction method (Larson et al. 2013), accounts for the linear bias caused by vertical motion of the sea surface. Later studies expanded on this approach with tidal harmonic analysis (Löfgren et al. 2014; Larson et al. 2017), or by directly estimating reflector height and its rate of change (Roussel et al. 2015). A more recent method, the Windowed Lomb-Scargle Periodogram (WinLSP) (Wang et al. 2019), combines moving-window frequency analysis with tropospheric corrections and a robust iteratively reweighted least squares (IRLS) regression scheme.

In this study, we introduce two further improvements. First, we adapt the h-rate correction to account for damping (decay) effects caused by sea surface roughness, reflectivity, and antenna gain patterns. In practice, the decaying

✉ Simon D. P. Williams
sdwil@noc.ac.uk

[1] Department of Geomatic Engineering, Yildiz Technical University, Istanbul, Turkey

[2] National Oceanography Centre, Liverpool, UK

Published online: 10 April 2026

amplitude of the SNR oscillations gives more influence to higher-amplitude epochs. We therefore generalize the h-rate correction by using amplitude-squared exponential weights, which leads to more reliable reflector height estimates under varying damping conditions. Second, we refine the robust IRLS strategy originally proposed by Wang et al. (2019). Instead of computing bisquare weights directly from raw residuals, we standardize the residuals using a robust MAD (Median Absolute Deviation) based scale estimate and apply a normalization so that the sum of the weights equals the number of observations. This adjustment preserves the numerical scale of the system across iterations, stabilizes convergence under diverse noise levels, and provides more consistent results across datasets.

The proposed refinements were first evaluated using simulated datasets representing extreme conditions, including high reflector h-rates and strong damping effects. These tests demonstrated that the damping-aware h-rate correction and the normalized IRLS framework retain accuracy and stability under such challenging scenarios. Subsequently, real GNSS observations from stations with different levels of surface roughness and damping were analyzed. The resulting sea level estimates were compared against near or co-located tide gauge measurements, which showed that the proposed improvements lead to more reliable and stable GNSS-IR sea level retrievals.

Methodology

This section describes the theoretical basis of GNSS-IR sea level estimation, the classical h-rate correction, and the WinLSP framework. We then introduce two methodological refinements: a damping-aware h-rate correction and a normalized IRLS strategy.

Static GNSS-IR model

In the classical GNSS-IR framework, the reflector height is assumed to remain constant during a satellite pass. The detrended SNR (dSNR) series can be expressed as:

$$dSNR\,(t) = A\cos\left(\frac{4\pi h}{\lambda}\sin E\,(t) + \phi\right) \tag{1}$$

where A is the oscillation amplitude, h is the static reflector height, λ is the signal wavelength, $E\,(t)$ is the satellite elevation angle, and ϕ is the initial phase.

In this model, the reflector height is retrieved by applying the Lomb-Scargle Periodogram (LSP) to the dSNR series. The peak frequency f_p of the LSP is related to the reflector height by:

$$h^{LSP} = f_p\lambda/2 \tag{2}$$

This static assumption is effective when the sea surface remains nearly constant within the duration of the arc. However, in tidal or storm-driven environments, the water surface often varies during the observation period, leading to systematic biases if uncorrected.

Height-rate correction.

Larson et al. (2013) showed that the static height assumption introduces a bias in the estimated reflector height when the sea surface changes during the SNR arc. The bias can be approximated as:

$$\delta h_{\dot{h}} \approx \dot{h}\frac{\overline{\tan E}}{\bar{\dot{E}}} \tag{3}$$

where $\dot{h}$ is the vertical rate of change of the reflector height, $\overline{\tan E}$ is the mean tangent of the elevation angle across the arc, and $\bar{\dot{E}}$ is the mean elevation rate. Accordingly, the corrected reflector height is obtained as:

$$h^{Corr} = h^{LSP} - \delta h_{\dot{h}} \tag{4}$$

with h^{LSP} denoting the raw height from the LSP peak frequency.

Although effective for moderate height changes, this correction is limited in practice. Two main issues can be noted. First, the approach assumes uniform weighting of the SNR samples across the arc, whereas in reality the signal amplitude varies due to damping, giving disproportionate influence to certain epochs. Second, the formulation requires knowledge of the height variation $\dot{h}$, which cannot be obtained directly. To overcome this, earlier studies first estimated static reflector heights and then applied either a fit to those values or a tidal harmonic model using the dominant tidal constituents (Löfgren et al. 2014). While these fits provide improved estimates of $\dot{h}$, they rely on post-processed daily time series and therefore remain unsuitable for near real-time applications.

Windowed Lomb-Scargle Periodogram (WinLSP) method

The limitations of classical h-rate correction motivated a series of developments aimed at directly solving the dynamic reflector height problem. Roussel et al. (2015) introduced the dynamic SNR method, where both instantaneous reflector height and its temporal change were estimated simultaneously using a least-squares approach. Larson et al. (2017) further advanced this direction by embedding the h-rate term directly within tidal harmonic analysis. Building on these efforts, Wang et al. (2019) consolidated the approach

into a more general framework by formulating the observation equations with tropospheric delay corrections included, and by introducing a robust IRLS adjustment scheme. Their method, later referred to as the WinLSP, provided a structured and broadly applicable model that has since become widely adopted for dynamic GNSS-IR sea level estimation.

In the WinLSP framework, the reflector height estimates derived from LSP are combined with tropospheric delay corrections and solved within a sliding window scheme. For a given satellite pass j within window w, the observation equation and its functional model can be written as:

$$y_{j,w} = h_{j,w}^{LSP} - \delta T_{j,w} = h_w + \dot{h}_w \left[\Delta t_j \frac{\overline{\tan(E_j)}}{\overline{\dot{E}_j}} + (t_{j,w} - t_w) \right] + r_{j,w} \tag{5}$$

where $h_{j,w}^{LSP}$ is the raw reflector height estimated from the LSP frequency, $\delta T_{j,w}$ represents the tropospheric correction following Williams and Nievinski (2017), h_w and $\dot{h}_w$ are the unknown reflector height and its temporal rate of change within window w, Δt_j is the time span of arc j, $\overline{\tan(E_j)}$ and $\overline{\dot{E}_j}$ are the mean tangent of elevation angle and mean elevation rate of arc j, $t_{j,w}$ is the mean epoch of arc j within window w, t_w is the reference epoch of window w, and $r_{j,w}$ denotes the residual. Stacking all observations within a window gives the adjustment system:

$$\mathbf{y}_w = \mathbf{A}_w \mathbf{x}_w + \mathbf{r}_w \tag{6}$$

where $\mathbf{y}_w$ is the vector of LSP-derived reflector heights corrected for tropospheric delay, $\mathbf{A}_w$ is the design matrix, and $\mathbf{x}_w = \begin{bmatrix} h_w & \dot{h}_w \end{bmatrix}^{\mathrm{T}}$, represents the unknown reflector height and its temporal rate of change within window w.

If all observations are assumed to have equal precision, the unknowns can be solved by ordinary least squares. However, as Wang et al. (2019) emphasized, GNSS-IR measurements often exhibit varying levels of precision due to geometry, multipath, and environmental conditions. To address this, they proposed a robust regression strategy based on IRLS procedure. In this scheme, each observation is assigned a weight w_j, updated iteratively as a function of the normalized residuals using a bisquare function. The process is repeated until changes in the parameter estimates between iterations fall below a predefined threshold. Thus, the final weighted least-squares solution is given by:

$$\widehat{\mathbf{x}}_w = \left({\mathbf{A}_w}^T \mathbf{W}_w \mathbf{A}_w \right)^{-1} {\mathbf{A}_w}^T \mathbf{W}_w \mathbf{y}_w \tag{7}$$

where $\mathbf{W}_w$ is the diagonal weight matrix obtained from the IRLS procedure. However, updating bisquare weights directly from raw residuals can result in unstable and inconsistent weighting when residual magnitudes differ across datasets.

Damping-aware height-rate correction

As shown in Eq. (3), the classical h-rate correction assumes uniform weighting of all epochs within the SNR arc. In practice, however, dSNR oscillations are attenuated due to sea surface roughness, reflectivity, and antenna gain patterns. This decay modifies the effective contribution of different elevation angles, with high-amplitude epochs having more influence than low-amplitude ones. The attenuation can be described by an exponential damping term defined as:

$$\alpha(E) = e^{-\Lambda k^2 \sin^2(E)} \tag{8}$$

where $k = 2\pi/\lambda$ is the wavenumber and Λ is a decay constant related to the scattering and roughness properties of the reflecting surface. Physically, $\alpha(E)$ represents the reduction of the multipath oscillation amplitude with elevation angle, such that larger elevation angles are associated with stronger damping. By incorporating squared damping weights into Eq. (3), the generalized h-rate correction for a given arc is expressed as:

$$\delta h_h = \dot{h} \frac{\sum_{i=1}^{n} {\alpha_i}^2 \tan(E_i)}{\sum_{i=1}^{n} {\alpha_i}^2 \dot{E}_i} = \dot{h} \frac{\sum_{i=1}^{n} e^{-2\Lambda k^2 \sin^2(E_i)} \tan(E_i)}{\sum_{i=1}^{n} e^{-2\Lambda k^2 \sin^2(E_i)} \dot{E}_i} \tag{9}$$

where i denotes the individual epochs within arc j, and n is the total number of epochs in that arc. This formulation ensures that the h-rate correction reflects the unequal influence of different elevation angles under signal attenuation. The effect is particularly important for arcs covering wide elevation ranges, where the decay of oscillations is more pronounced. It should be noted, however, that this formulation assumes a monotonic, elevation-dependent amplitude decay. At sites with a complex multipath environment beyond the water surface, amplitude variations may deviate from this pattern, potentially reducing the effectiveness of the damping-aware correction.

In the estimation procedure, it is assumed that all arcs within the same analysis window share a common damping parameter Λ. For each arc, arc-specific sine and cosine amplitudes (A_s, A_c) – corresponding to the harmonic components of the dSNR model – are solved simultaneously, while a single Λ is estimated for the entire window. This is achieved using the variable projection method, in which the linear amplitude parameters are eliminated and the nonlinear damping parameter is optimized directly. The resulting Λ is used to construct the exponential weights in the damping-aware h-rate correction. In contrast to previous WinLSP implementations, the coefficient of $\dot{h}$ is here computed using

these revised damping-aware weights rather than the classical average term in Eq. (3). Accordingly, the elements of the design matrix $\mathbf{A}$ in Eq. (6) are updated using the weighted averages given in Eq. (9), so that the observation model in Eq. (5) inherently reflects the damping-aware correction.

Normalized IRLS strategy.

In the WinLSP framework, robust estimation is achieved through an IRLS procedure in which observation weights are updated at each iteration. In the original formulation, bisquare weights were computed directly from raw residuals. This approach may lead to inconsistent weighting behavior when the magnitude of residuals varies across datasets, since large residuals can collapse weights while small residuals may yield nearly uniform weighting. To address this, we adopt a normalized bisquare weighting strategy. In each IRLS iteration k, the residual vector is defined as $\mathbf{r}^{(k)} = \left[r_1^{(k)}, r_2^{(k)}, \ldots, r_N^{(k)}\right]$, where $r_i^{(k)}$ is the residual for the i-th observation. The scale of the residuals is estimated using the MAD:

$$\widehat{\sigma} = 1.4826 \times median\left(\left|r_i^{(k)} - median\left(\mathbf{r}^{(k)}\right)\right|\right) \tag{10}$$

Each residual is standardized as:

$$u_i^{(k)} = \frac{r_i^{(k)}}{c\widehat{\sigma}} \tag{11}$$

where c is a tuning constant, typically selected as $c = 4.685$ (Woolrich 2008), defining the inlier threshold under the assumption of normally distributed residuals. The bisquare weight for the i-th observation is then computed as:

$$b_i{}^{(k)} = \begin{cases} \left(1 - \left(u_i{}^{(k)}\right)^2\right)^2, & \left|u_i{}^{(k)}\right| \leq 1 \\ 0, & otherwise \end{cases} \tag{12}$$

To preserve the overall scale of the weight matrix throughout the IRLS process, the bisquare weights are normalized such that their sum equals the number of observations (N):

$$\tilde{b}_i^{(k)} = \frac{b_i{}^{(k)}}{\sum_{j=1}^{N} b_j{}^{(k)}} N \tag{13}$$

These normalized bisquare weights $\tilde{b}_i^{(k)}$ are then applied as the diagonal elements of the weight matrix $\mathbf{W}^{(k)}$ in the weighted least squares system.

Simulation-based evaluation

To evaluate the impact of the proposed damping-aware h-rate correction, controlled simulations were performed using the MPSIM open-source multipath simulator (Nievinski and Larson 2014a). Synthetic dSNR signals were generated for elevation angles between 2° and 15°, assuming an initial reflector height of 10 m and one-hour arc length at the L1 frequency. The reflector h-rate varied between 0 and 2 m/h, and the surface roughness standard deviation between 0 and 0.75 m. The damping parameter Λ was set proportional to the square of surface standard deviation ($\Lambda = 0.5 \times (Surface\,Std)^2$), consistent with the formulation in Nievinski and Larson (2014b).

Reflector heights were first estimated from the LSP peak frequency and then corrected using both the classical h-rate correction, and the damping-aware correction. Errors were computed as the difference between the estimated and the true reflector height at the arc midpoint, expressed in cm.

Figure 1 shows the simulation results. The upper panels present the error distributions of the classical and damping-aware h-rate corrections as a function of reflector h-rate and surface roughness. The lower panels display the error variation with surface roughness at a fixed h-rate of 0.5 m/h, and with h-rate at a fixed surface roughness of 0.25 m.

The results demonstrate that the classical correction exhibits increasing negative biases as both reflector height rate and surface roughness increase. By contrast, the damping-aware correction significantly reduces these systematic errors, particularly under stronger damping conditions and across wider elevation ranges. These results indicate that accounting for damping effects leads to more stable and accurate reflector height estimates in simulated environments.

Performance assessment with real GNSS-IR data

GNSS data and processing setup

The performance of the proposed methodology was further examined using one-month GNSS datasets from three coastal stations equipped with co-located tide gauges. The selected sites (ALTG—Liverpool, UK; BRST—Brest, France; and SHRN—Sheerness, UK) represent diverse tidal environments and reflector height ranges. Reference reflector heights were obtained from the PSMSL GNSS-IR portal, while tide gauge records were sourced from the IOC database (Flanders Marine Institute (VLIZ) and Intergovernmental Oceanographic Commission (IOC) 2021). For

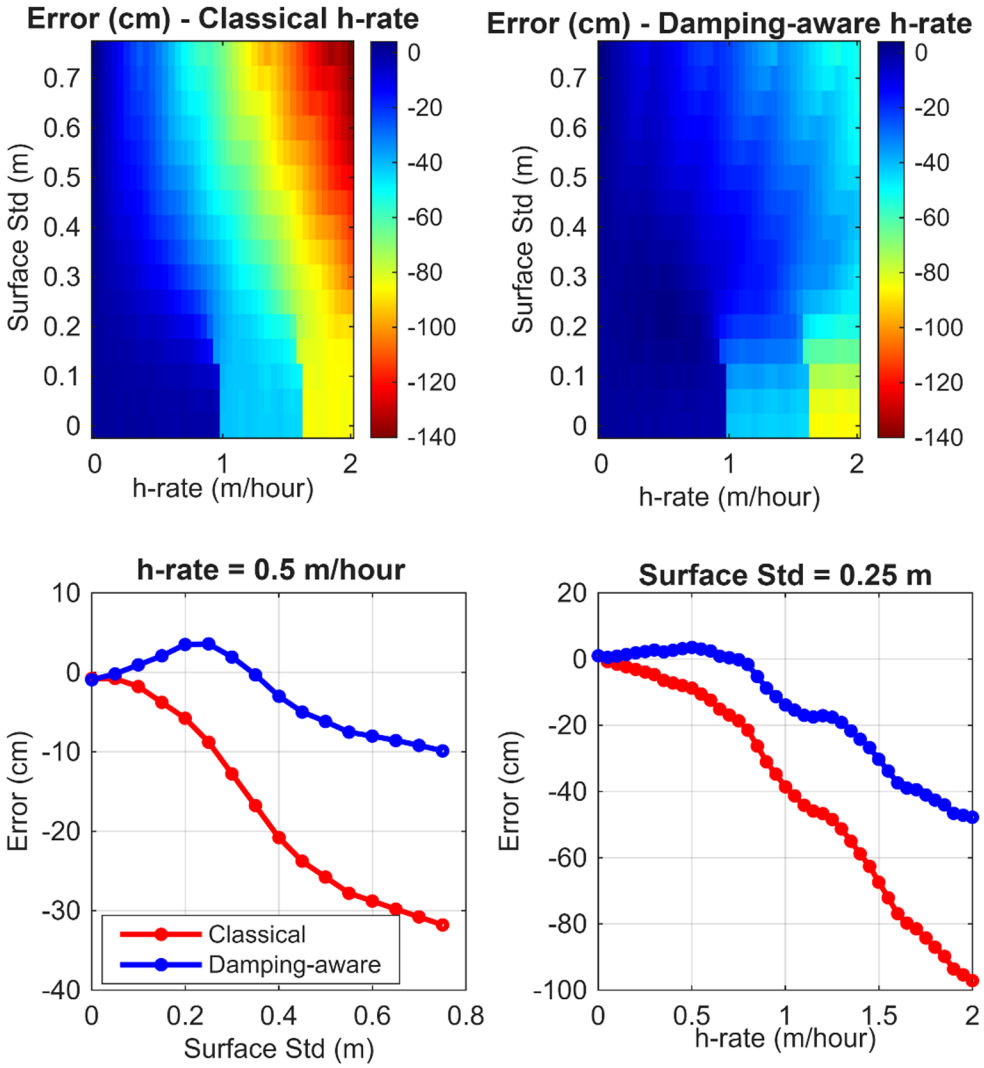

Fig. 1 Simulation results comparing classical and damping-aware h-rate corrections under varying reflector h-rates and surface roughness conditions

Table 1 Overview of the GNSS sites, corresponding tide gauge sites, average reflector heights, analysis periods, and angle ranges

GNSS Site ID	TG Site ID	RH (m)	Period	Elevation range (°)	Azimuth range (°)
ALTG	VG (Alfred lock)	10.447	1–31 Jan 2025	2–30	0–160
BRST	Bres	16.803	13 Feb–14 Mar 2025	10–30	130–330
SHRN	Shee	8.919	6 Mar–7 Apr 2025	2–30	180–300

BRST and SHRN, IOC records from co-located tide gauges were used directly. At ALTG, however, the co-located radar gauge at Alfred Lock was not operational during the analysis period. A virtual tide gauge (VG) record was therefore constructed by combining predicted tides from 700 days of 1-min radar gauge data with non-tidal residuals derived from 34 years of 15-min records at the nearby Gladstone Dock gauge (4.91 km downstream). All three stations are equipped with Trimble Alloy receivers; ALTG and SHRN use TRM159900.00 antennas with SCIS radomes, while BRST operates a TRM57971.00 antenna without a radome.

At ALTG, the tidal range is about 8 m, and the reflector height LSP search interval was set between 2.5 and 18.5 m with 0.01 m precision. At BRST, the expected tidal range is 8 m, with bounds of 9–25 m. For SHRN, the tidal range reaches approximately 7 m, and the interval was defined as 2–16 m. A summary of the analysis periods and elevation-azimuth ranges is provided in Table 1.

For the WinLSP analysis, a window length of 60 min and a window shift of 10 min were used. Quality control was applied by requiring a minimum peak-to-background noise ratio (PBNR) of 3 and minimum elevation range 3°. Due to the weak dSNR oscillations, S1W and S2W observations were excluded from the analysis. The analysis included observations from four GNSS constellations: GPS (G), GLONASS (R), Galileo (E), and BeiDou (C). The

Table 2 GNSS constellations and SNR observables used at each station

Station	GPS	GLONASS	Galileo	BeiDou
ALTG	S1C, S1X, S2X, S5X	S1C, S1P, S2C, S2P, S3X	S1X, S5X, S7X, S8X	S2I, S5X, S6I, S7D, S7I
BRST	S1C, S2X, S5X	S1C, S1P, S2C, S2P	S1X, S5X, S6X, S7X, S8X	S1X, S2I, S5X, S6I, S7I
SHRN	S1C, S1X, S2X, S5X	S1C, S1P, S2C, S2P, S3X	S1X, S5X, S6X, S7X, S8X	S1X, S2I, S5X, S6I, S7I

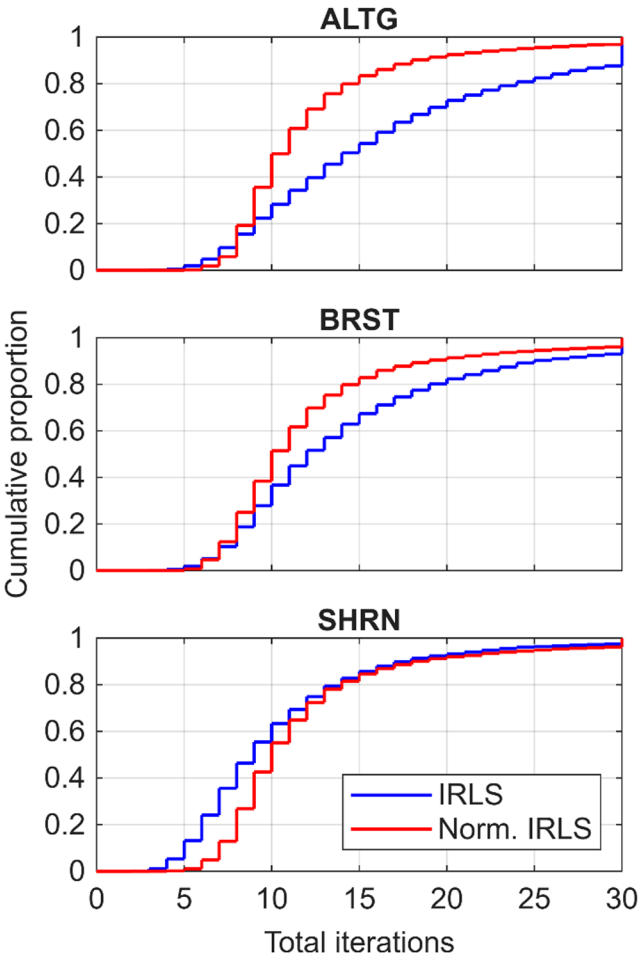

Fig. 2 Cumulative distribution of IRLS iteration counts for the original IRLS and normalized IRLS strategies at ALTG, BRST, and SHRN over the full one-month analysis periods

specific SNR observables used at each station are listed in Table 2. For the estimation of tropospheric height bias, we computed the differential delays between the antenna and the reflection surface using the GPT2w model for meteorological parameters (Böhm et al. 2015). The Saastamoinen (1972) and Askne and Nordius (1987) formulations were applied for hydrostatic and wet zenith delays, respectively, together with the VMF1 mapping function for slant delay calculations (Boehm et al. 2006).

Table 3 Iteration count distribution for the original IRLS and normalized IRLS strategies at each station

Station	Method	1–10 (%)	11–20 (%)	21–30 (%)
ALTG	IRLS	28.2	44.6	27.2
	Norm. IRLS	50.0	42.5	7.5
BRST	IRLS	36.7	45.6	17.7
	Norm. IRLS	51.4	39.9	8.6
SHRN	IRLS	63.3	29.9	6.8
	Norm. IRLS	55.1	36.9	8.0

Convergence analysis of the IRLS strategies

To evaluate the convergence properties of the normalized IRLS strategy, the iteration counts of both the original and normalized IRLS were compared across all three stations over the full one-month analysis periods. A maximum of 30 iterations was set for both methods, with convergence declared when changes in parameter estimates between successive iterations fell below 10^{-6}, a threshold sufficiently small to ensure numerical stability.

Figure 2 presents the cumulative distribution of iteration counts for each station. At ALTG and BRST, the normalized IRLS converges notably faster, with a higher proportion of windows reaching convergence within fewer iterations. At SHRN, both methods exhibit comparable convergence behavior. The corresponding iteration count distributions are summarized in Table 3.

Overall, the normalized IRLS reduces the occurrence of high-iteration windows, particularly at stations where residual magnitudes vary more widely. This supports the stabilizing effect of the MAD-based residual scaling and weight normalization introduced in the proposed strategy.

Retrieval accuracy and impact of refinements

The resulting sea level estimates from the WinLSP approach and from the proposed methodology were compared against co-located tide gauge observations. Figure 3 illustrates the one-month time series for each site, while Fig. 4 presents the comparisons with tide gauge data, the upper panels show scatter plots of GNSS-IR versus tide gauge sea levels, and the lower panels display the corresponding Van de Casteele diagrams.

In the time series, both methods capture overall tidal variability. However, the proposed method reduces systematic deviations, particularly during periods of strong tidal dynamics. The scatter plots further show that results from the proposed method are more tightly clustered along the 1:1 line, especially at ALTG and SHRN, indicating reduced bias. The Van de Casteele diagrams show that the classical

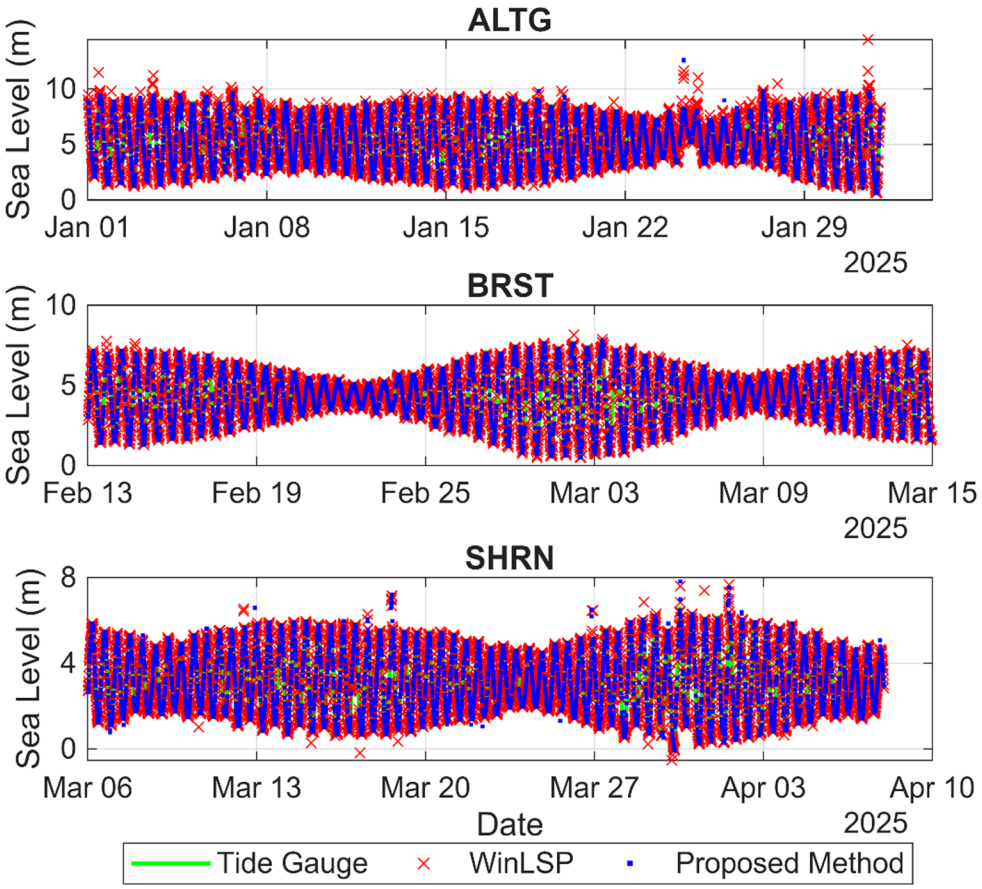

Fig. 3 Time series of sea level estimates from WinLSP and the proposed method with tide gauge records at ALTG, BRST, and SHRN stations

h-rate correction can introduce positive sea level biases, consistent with the negative reflector height bias observed in simulations, whereas the proposed method mitigates these effects, yielding errors more tightly centered around zero.

To assess the individual and combined contributions of each refinement, four configurations were evaluated: the baseline WinLSP with uniform h-rate correction and original IRLS (WinLSP), WinLSP with damping-aware h-rate correction only (WinLSP+D), WinLSP with normalized IRLS only (WinLSP+N), and the full proposed method combining both refinements (Proposed method). The quantitative results are summarized in Table 4.

The relative contribution of each refinement varies across stations. At ALTG, both refinements individually reduce the RMS error, but the normalized IRLS has the larger effect, decreasing the RMS from 47.5 cm to 26.5 cm, while the damping-aware correction alone reduces it to 34.9 cm. At BRST, the improvement is driven predominantly by the normalized IRLS, which reduces the RMS from 21.9 to 15.6 cm, whereas the damping-aware correction alone yields only a marginal change. At SHRN, the damping-aware correction is the dominant contributor, reducing the RMS from 24.2 to 18.6 cm, while the normalized IRLS alone achieves 19.7 cm. In all three cases, the combined configuration achieves the lowest or near-lowest RMS errors, indicating that the two refinements address complementary sources of error. The number of estimations (NoE) remains comparable across all configurations, confirming that the improvements are not due to excessive data rejection.

Performance during storm surges and high sea states

To examine the behavior of the methods under challenging sea state conditions, the GNSS-IR estimation errors at ALTG were analyzed alongside non-tidal residual data from the British Oceanographic Data Centre (BODC). The BODC residuals represent the difference between observed and predicted tidal water levels and reflect meteorological influences such as wind and atmospheric pressure variations on sea level. Periods of elevated non-tidal activity were identified as epochs where the absolute residual exceeded 0.50 m.

Figure 5 shows the non-tidal residual record alongside the GNSS-IR estimation errors for both methods. The most prominent event occurred between 23 and 28 January 2025, during which residuals exceeded 1.5 m. This period coincides with a visible increase in scatter for both methods, though the proposed method maintains notably smaller deviations.

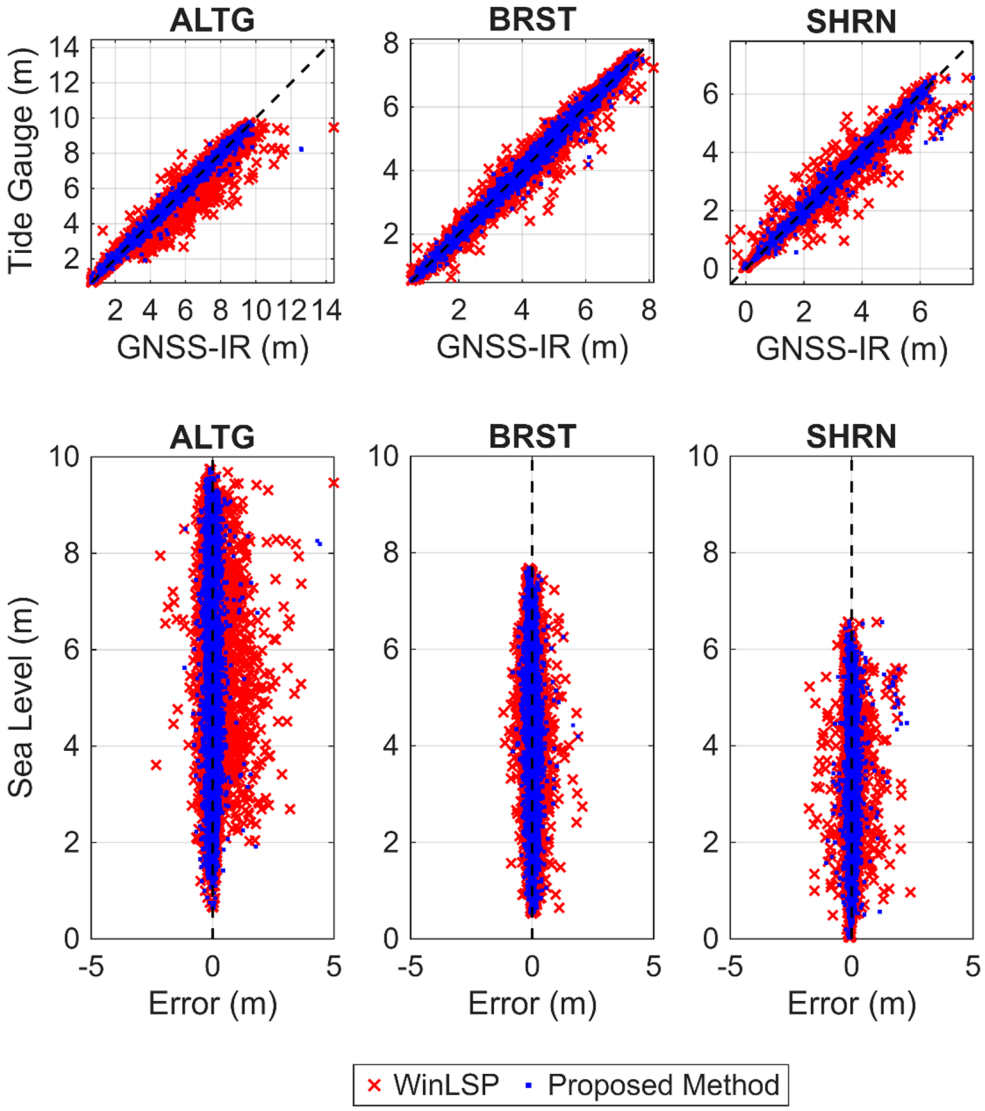

Fig. 4 Scatter plots and Van de Casteele diagrams comparing GNSS-IR sea level estimates from WinLSP and the proposed method with tide gauge observations

Table 4 Statistical performance of GNSS-IR sea level retrievals for four configurations at each station, based on a 60-minute window length and 10-min window shift. D: Damping-aware h-rate correction; N: normalized IRLS

Site	Method	Corr. (%)	RMS (cm)	NoE	<10 cm	10–20 cm	>20 cm
ALTG	WinLSP	98.1	47.5	4316	1785 (41.4%)	953 (22.1%)	1578 (36.6%)
	WinLSP+D	98.9	34.9	4312	2127 (49.3%)	1130 (26.2%)	1055 (24.5%)
	WinLSP+N	99.4	26.5	4212	2028 (48.1%)	1149 (27.3%)	1035 (24.6%)
	Proposed method	99.6	21.6	4241	2200 (51.9%)	1162 (27.4%)	879 (20.7%)
BRST	WinLSP	99.1	21.9	4307	2417 (56.1%)	995 (23.1%)	895 (20.8%)
	WinLSP+D	99.1	21.3	4305	2454 (57.0%)	997 (23.2%)	854 (19.8%)
	WinLSP+N	99.5	15.6	4296	2625 (61.1%)	1059 (24.7%)	612 (14.2%)
	Proposed method	99.5	15.5	4299	2664 (62.0%)	1041 (24.2%)	594 (13.8%)
SHRN	WinLSP	98.7	24.2	4621	3021 (65.4%)	948 (20.5%)	652 (14.1%)
	WinLSP+D	99.3	18.6	4637	3422 (73.8%)	811 (17.5%)	404 (8.7%)
	WinLSP+N	99.2	19.7	4574	3018 (66.0%)	988 (21.6%)	568 (12.4%)
	Proposed method	99.4	17.0	4591	3370 (73.4%)	841 (18.3%)	380 (8.3%)

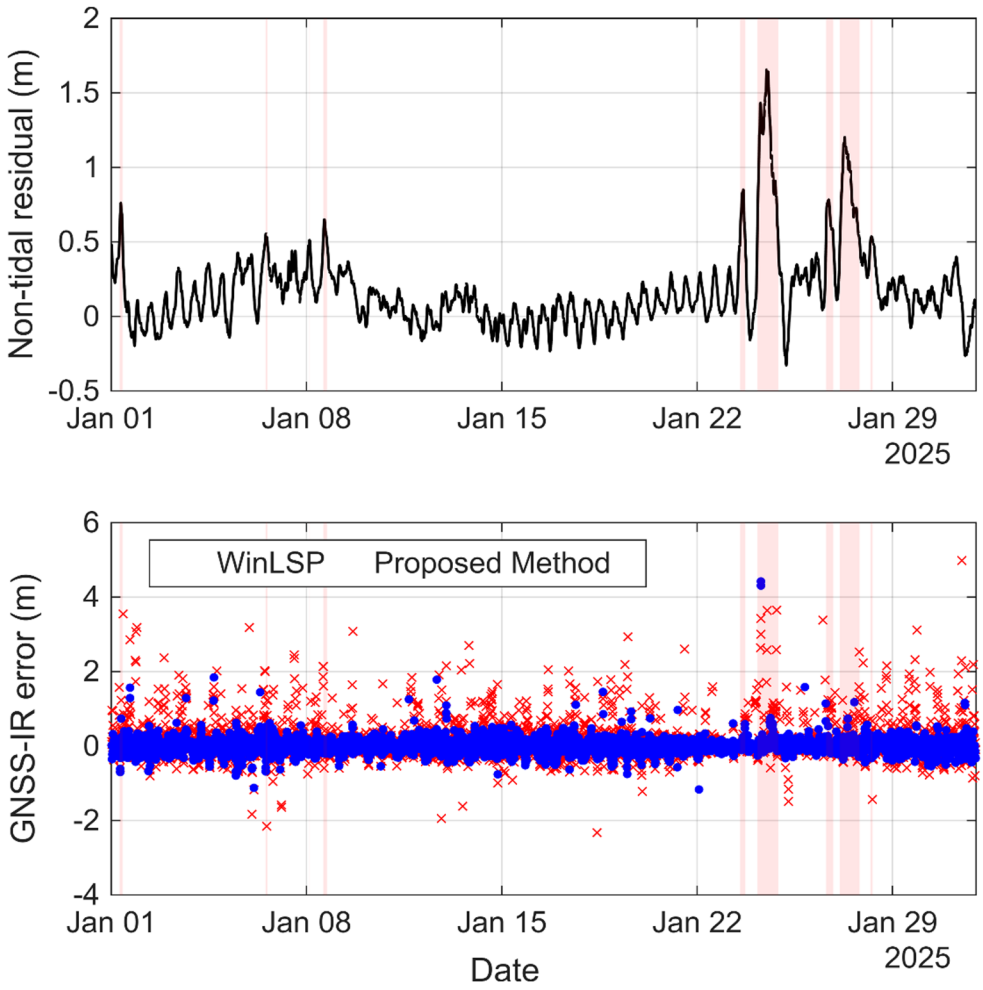

Fig. 5 Non-tidal meteorological residuals at ALTG derived from BODC tide gauge records (upper panel) and GNSS-IR estimation errors for WinLSP and the proposed method (lower panel) during January 2025. Shaded regions indicate periods where the absolute residual exceeds 0.50 m

Table 5 RMS errors of GNSS-IR sea level retrievals at ALTG during periods of elevated and non-elevated non-tidal residuals

Period	Method	RMS (cm)	NoE
Full analysis	WinLSP	47.5	4316
	Proposed method	21.6	4241
Elevated periods	WinLSP	70.5	300
	Proposed method	43.1	274
Non-elevated periods	WinLSP	45.4	4016
	Proposed method	19.3	3967

Elevated periods are defined as epochs where the absolute meteorological residual from the BODC tide gauge record exceeds 0.50 m

The RMS errors for elevated and non-elevated periods are summarized in Table 5. During elevated periods, the RMS error increases for both methods compared to the full analysis period, rising from 47.5 to 70.5 cm for WinLSP and from 21.6 to 43.1 cm for the proposed method. However, the proposed method still reduces the RMS by approximately 39% relative to WinLSP during these periods. Outside elevated periods, the proposed method achieves an RMS of 19.3 cm, representing a 57% improvement over WinLSP.

The degraded performance during high sea states can be attributed to several factors. Rapid and non-linear sea level changes within analysis windows violate the linear h-rate assumption underlying both methods. Additionally, increased sea surface roughness amplifies signal scattering, leading to noisier SNR observations and less reliable spectral estimates. Despite these challenges, the proposed method consistently outperforms WinLSP across both calm and disturbed conditions, demonstrating its robustness under varying sea states.

It should be noted, however, that GNSS-IR methods including the one proposed here are inherently limited in extreme scenarios such as tsunamis, where sea level changes can occur on timescales shorter than typical satellite arc durations. Under such conditions, the windowed estimation framework may not capture the full dynamics of the event. The present analysis demonstrates the method's applicability to periods of elevated non-tidal sea level variability, but its extension to more extreme and rapid phenomena would require further investigation.

Conclusion

We introduced two refinements to the WinLSP framework for GNSS-IR sea level estimation: a damping-aware height-rate correction and a normalized IRLS strategy. Simulation experiments showed that the damping-aware height-rate correction reduces systematic biases under challenging conditions, including strong damping and high reflector height rates. Real data analyses from three coastal stations confirmed the improvements, with RMS errors reduced from 47.5 to 21.6 cm at ALTG, from 21.9 to 15.5 cm at BRST, and from 24.2 to 17.0 cm at SHRN, while correlations with tide gauge records exceeded 99%. An evaluation of the individual refinements showed that their relative contributions are site-dependent, with the normalized IRLS being more effective at stations with larger residual variability and the damping-aware correction providing greater benefit where elevation-dependent amplitude decay is more pronounced. The normalized IRLS also demonstrated faster convergence compared to the original IRLS, particularly at stations with diverse noise characteristics. An analysis of GNSS-IR performance during periods of elevated non-tidal sea level variability at ALTG further showed that the proposed method maintains its advantage under high sea state conditions, though with increased errors for both methods. By explicitly accounting for damping effects and adopting a normalized weighting scheme for IRLS, we enhanced both the robustness and reliability of GNSS-IR sea level retrievals. While this study focused on exponential amplitude decay, future work could investigate more complex, non-exponential amplitude variations observed at coastal stations where multipath signal strength fluctuates irregularly with elevation angle.

Acknowledgements The authors would like to thank F. G. Nievinski and K. M. Larson for developing the open-source MPSIM multipath simulator, which was used to generate simulated dSNR signals.

Author contributions C. A. developed the methodology, performed the simulations and data analyses, and drafted the manuscript. S.W. identified the damping-related effect, contributed substantially to the methodological development, and provided detailed feedback on the analyses and manuscript. Both S. W. and N. T. supervised the research and reviewed the manuscript.

Funding Cemali Altuntas is supported by The Scientific and Technological Research Council of Turkey (TUBITAK) 2214/A International Doctoral Research Fellowship Programme (Grant No:1059B142401170).

Data availability GNSS data for BRST station were obtained from the CDDIS archive (https://cddis.nasa.gov/archive/gnss). GNSS data for ALTG and SHRN stations were provided by the National Oceanography Centre (NOC) and are available at Zenodo (DOI: https://doi.org/10.5281/zenodo.17224582). Tide gauge data were obtained from the IOC Sea Level Station Monitoring Facility (http://www.ioc-sealevelmonitoring.org). Non-tidal residual data used for the storm surge analys is were obtained from the BODC UK National Tide Gauge Network (https://www.bodc.ac.uk/data/hosted_data_systems/sea_level/uk_tide_gauge_network/processed).

Declarations

Competing interests The authors declare no competing interests.

References

Altuntas C, Tunalioglu N (2020) Estimation performance of soil moisture with GPS-IR method. Sigma J Eng Nat Sci 38(4):2217–2230

Altuntas C, Iban MC, Şentürk E, Durdag UM, Tunalioglu N (2022) Machine learning-based snow depth retrieval using GNSS signal-to-noise ratio data. GPS Solut 26(4):117. https://doi.org/10.1007/s10291-022-01307-2

Askne J, Nordius H (1987) Estimation of tropospheric delay for microwaves from surface weather data. Radio Sci 22(3):379–386. https://doi.org/10.1029/RS022i003p00379

Boehm J, Werl B, Schuh H (2006) Troposphere mapping functions for GPS and very long baseline interferometry from European Centre for Medium-Range Weather Forecasts operational analysis data. J Geophys Res Solid Earth 111(B2):B02406. https://doi.org/10.1029/2005JB003629

Böhm J, Möller G, Schindelegger M, Pain G, Weber R (2015) Development of an improved empirical model for slant delays in the troposphere (GPT2w). GPS Solut 19:433–441. https://doi.org/10.1007/s10291-014-0403-7

Flanders Marine Institute (VLIZ), Intergovernmental Oceanographic Commission (IOC) (2021) Sea level station monitoring facility. VLIZ, Oostende, Belgium. http://www.ioc-sealevelmonitoring.org https://doi.org/10.14284/482

Larson KM, Small EE, Gutmann ED, Bilich AL, Braun JJ, Zavorotny VU (2008) Use of GPS receivers as a soil moisture network for water cycle studies. Geophys Res Lett 35(24):L24405. https://doi.org/10.1029/2008GL036013

Larson KM, Gutmann ED, Zavorotny VU, Braun JJ, Williams MW, Nievinski FG (2009) Can we measure snow depth with GPS receivers? Geophys Res Lett 36(17):L17502. https://doi.org/10.1029/2009GL039430

Larson KM, Ray RD, Nievinski FG, Freymueller JT (2013) The accidental tide gauge: a GPS reflection case study from Kachemak Bay, Alaska. IEEE Geosci Remote Sens Lett 10(5):1200–1204. https://doi.org/10.1109/LGRS.2012.2236075

Larson KM, Ray RD, Williams SDP (2017) A 10-year comparison of water levels measured with a geodetic GPS receiver versus a conventional tide gauge. J Atmos Ocean Technol 34(2):295–307. https://doi.org/10.1175/JTECH-D-16-0101.1

Löfgren JS, Haas R, Scherneck HG (2014) Sea level time series and ocean tide analysis from multipath signals at five GPS sites in different parts of the world. J Geodyn 80:66–80. https://doi.org/10.1016/j.jog.2014.02.012

Nievinski FG, Larson KM (2014a) An open source GPS multipath simulator in Matlab/Octave. GPS Solutions 18:473–481. https://doi.org/10.1007/s10291-014-0370-z

Nievinski FG, Larson KM (2014b) Inverse modeling of GPS multipath for snow depth estimation—Part I: formulation and simulations. IEEE Trans Geosci Remote Sens 52(10):6555–6563. https://doi.org/10.1109/TGRS.2013.2297681

Regmi A, Leinonen ME, Pärssinen A, Berg M (2022) Monitoring sea ice thickness using GNSS-interferometric reflectometry. IEEE Geosci Remote Sens Lett 19:1–5. https://doi.org/10.1109/LGRS.2022.3198189

Roggenbuck O, Reinking J, Lambertus T (2019) Determination of significant wave heights using damping coefficients of attenuated GNSS SNR data from static and kinematic observations. Remote Sens 11(4):409. https://doi.org/10.3390/rs11040409

Roussel N, Ramillien G, Frappart F, Darrozes J, Gay A, Biancale R, Striebig N, Hanquiez V, Bertin X, Allain D (2015) Sea level monitoring and sea state estimate using a single geodetic receiver. Remote Sens Environ 171:261–277. https://doi.org/10.1016/j.rse.2015.10.011

Saastamoinen J (1972) Atmospheric correction for the troposphere and stratosphere in radio ranging satellites. In: Henriksen SW, Mancini A, Chovitz BH (eds) The use of artificial satellites for geodesy, vol 15. American Geophysical Union, Washington, DC, pp 247–251. https://doi.org/10.1029/GM015p0247.

Wang X, He X, Zhang Q (2019) Evaluation and combination of quad-constellation multi-GNSS multipath reflectometry applied to sea level retrieval. Remote Sens Environ 231:111229. https://doi.org/10.1016/j.rse.2019.111229

Williams SDP, Nievinski FG (2017) Tropospheric delays in ground-based GNSS multipath reflectometry—experimental evidence from coastal sites. J Geophys Res Solid Earth 122(3):2310–2327. https://doi.org/10.1002/2016JB013612

Woolrich M (2008) Robust group analysis using outlier inference. NeuroImage 41(2):286–301. https://doi.org/10.1016/j.neuroimage.2008.02.042

Cemali Altuntas is a research assistant at Yildiz Technical University. He received his B.Sc., M.Sc., and Ph.D. degrees in Geomatics Engineering, with his doctoral research focusing on GNSS Interferometric Reflectometry (GNSS-IR). He was a visiting researcher at the National Oceanography Centre, Liverpool, UK. His research interests include environmental monitoring applications, particularly sea-level estimation using GNSS-IR, as well as precise positioning techniques and advanced GNSS signal processing.

Simon D. P. Williams has a Ph.D. in Geodetic Geophysics from Durham University, United Kingdom. He worked at Scripps Institution of Oceanography before moving to the National Oceanography Centre. His research interests include stochastic modelling of time series, sea level and vertical land motion and the development of GNSS-IR.

Nursu Tunalioglu received her Ph.D. degree in geomatic engineering from Yildiz Technical University, Istanbul, Turkey, in 2011. She is currently working as a full professor at the same university. Her research interests include engineering surveys, highway planning, GNSS and high-accurate GNSS positioning, and GNSS-IR.